

# On the importance of catalysis in photocatalysis: Triggering of photocatalysis at well-defined anatase TiO<sub>2</sub> crystals through facet-specific deposition of oxygen reduction cocatalyst

Christiane Adler,<sup>a</sup> Dariusz Mitoraj,<sup>a</sup> Igor Krivtsov,<sup>a</sup> Radim Beranek<sup>a\*</sup>

<sup>a</sup> Institute of Electrochemistry, Ulm University, Albert-Einstein-Allee 47, 89081, Ulm, Germany

\* Corresponding author: E-mail: [radim.beranek@uni-ulm.de](mailto:radim.beranek@uni-ulm.de)

*Keywords:* photocatalysis, platinum nanoparticles, water depollution, oxygen reduction, charge separation

## ABSTRACT

Well-defined anatase TiO<sub>2</sub> crystals with co-exposed {101} and {001} facets represent a promising platform for fundamental studies in photocatalysis and for the development of novel photocatalytic systems exhibiting higher than usual quantum efficiencies. Herein, we present protocols enabling the photoreductive deposition of Pt nanoparticles onto anatase TiO<sub>2</sub> micro-sized (1-3 μm) crystals prepared by hydrothermal growth in fluoride-containing solutions to be carried out either facet-selectively (on {101} facets only) or facet non-selectively (on both {101} and {001} facets). The photocatalytic behavior of resulting photocatalysts is studied using investigations of oxidative photodegradation of a test pollutant (4-chlorophenol, 4-CP), photocurrent measurements, and kinetic analysis of the open-circuit photopotential decay. We demonstrate that the deposition of Pt nanoparticles effectively triggers the photocatalytic degradation of 4-CP at anatase crystals which are otherwise completely inactive. The role of Pt in triggering the photocatalysis is demonstrated to consist chiefly in the catalytic enhancement of the reaction rate of oxygen reduction by photogenerated electrons. Only platinized {101} facets contribute to photocatalysis, whereas the {001} facets, in the literature often referred to as “highly reactive”, are even after platinization completely inactive, most likely due to (1 × 4) surface reconstruction upon the heat treatment necessary to decrease the amount of surface fluorides. Based on our results, we highlight the eminent role of efficient surface catalysis for effective charge separation, and provide specific design rules for further development of photocatalysts with high quantum efficiencies.

## I. INTRODUCTION

Light-driven heterogeneous photocatalysis is potentially one of the most attractive techniques for driving useful redox transformations like decontamination of water and air from toxic organic contaminants, hydrogen evolution from water or selective syntheses of high-value compounds from low-value chemical feedstock with minimum input of energy and using easily available reagents like water or oxygen.<sup>1-8</sup> However, the real life applications of photocatalysis are still rather scarce, in particular due to very low quantum

efficiencies of most photocatalytic reactions. This is true also for an archetypal photocatalyst, titanium dioxide, a wide bandgap (3.0-3.2 eV) material that absorbs efficiently UV part of solar light and excels by its low cost, stability against photocorrosion, and low toxicity.<sup>1,9,10</sup> While the anatase phase of TiO<sub>2</sub> is often found to be photocatalytically more active than rutile TiO<sub>2</sub>,<sup>11-13</sup> the typically reported quantum yields of anatase TiO<sub>2</sub> are in the range of few per cent,<sup>14,15</sup> meaning that only a small fraction of photogenerated electrons and holes can avoid recombination and induce desired redox reactions at the photocatalyst surface. It should be noted that such poor quantum yields in photocatalysis are in stark contrast to quantum conversion efficiencies of ~100 % typically found in conventional solar energy converters like silicon solar cells. This obviously shows that typical photocatalysts are far from being optimized, which makes a search for more advanced design rules mandatory. Owing to the ground-breaking work of Max Lu *et al.*,<sup>16</sup> well-defined anatase TiO<sub>2</sub> crystals with co-exposed {101} and {001} facets have become available more than a decade ago and have attracted a lot of interest of scientific community, motivated mainly by two reasons. Firstly, the very presence of “highly reactive” {001} facets, typically absent in normally grown bipyramidal anatase crystals, was believed to be highly beneficial for photocatalysis.<sup>16-19</sup> Secondly, anatase TiO<sub>2</sub> crystals with co-exposed {101} and {001} were suggested to exhibit anisotropic transport of photogenerated charges, electrons to {101} and holes to {001} facets, which should lead to enhanced charge separation.<sup>20-27</sup> As an explanation for this anisotropy, both bulk properties (*e.g.*, anisotropic effective mass of electrons and holes)<sup>26</sup> and formation of a “surface heterojunction” at the interface of {101} and {001}<sup>25,27,28</sup> have been proposed. However, the experimental evidence for the anisotropic charge separation and its nature is not conclusive,<sup>29</sup> and the results of photocatalytic studies with anatase crystals exposing large amounts of {001} facets are also rather controversial.<sup>18,19,21,30,31</sup>

The scope of this paper is threefold. Firstly, we establish protocols for photodeposition of Pt nanoparticles, a prototypical cocatalyst in TiO<sub>2</sub> photocatalysis,<sup>32-37</sup> onto well-defined anatase crystals either facet-selectively, or facet non-selectively, and demonstrate that the platinization triggers photocatalytic degradation of a test organic pollutant at {101} crystal facets. Secondly, we provide conclusive experimental evidence for the catalysis of oxygen reduction as the key mechanistic aspect responsible for turning on the photocatalytic activity. Finally, we discuss the implications of our results for understanding the limitations of charge separation in photocatalysis, and provide some specific design rules for fabrication of advanced photocatalysts with improved quantum efficiency.

## II. EXPERIMENTAL

### A. Synthesis of anatase TiO<sub>2</sub> crystals with well-defined {001} and {001} facets

We adapted a protocol reported by Pan *et al.*<sup>30</sup> In a typical synthesis, 480 mg (3 mmol) of titanium oxysulfate was dissolved in 28.8 mL of deionized water and 1.8 mL of 50 vol% HF and was transferred into a Teflon-lined

autoclave. The autoclave was heated for 24 h at 180 °C and then cooled down to room temperature (RT). The crystals were collected by centrifugation, washed three times with distilled water and then dried at RT. In order to partially remove the surface fluorides, the powder was heated at 450 °C or 600 °C (gradient 5 K/min) for 2 h.

### **B. Photodeposition of platinum nanoparticles onto anatase TiO<sub>2</sub> crystals**

In a typical photodeposition procedure, 200 mg of anatase TiO<sub>2</sub> powder was dispersed in a mixture of 18 mL distilled water and 2 mL methanol, and then sonicated for 5 min. If not stated otherwise, 3.6 mg of hexachloroplatinic acid hexahydrate (H<sub>2</sub>PtCl<sub>6</sub> · 6H<sub>2</sub>O) was added, and the dispersion was irradiated for 1 h with the Ushio 150 W Xe lamp in a light-condensing lamp housing (LOT-Oriel GmbH); the irradiation intensity was ~1 sun. After successful deposition of platinum, the powder was washed three times with distilled water and dried at 80 °C overnight. A greyish powder with a yield of 95% could be obtained. This procedure resulted in actual Pt content of ca. 1 wt%, as determined by inductively coupled plasma atomic emission spectrometry (ICP-AES).

### **C. Sample characterization.**

XRD. X-ray diffraction (XRD) patterns were recorded using an X-ray diffractometer (Stoe Stadi P) with Cu K<sub>α1</sub> as X-ray source and a scan time of 15 minutes.

Raman spectroscopy. Raman spectra were measured with a Renishaw inVia™ Raman-dual-laser system equipped with a Leica DM 2500 microscope. Nd:YAG-Laser (532 nm, 50 mW) and He-Ne laser (633 nm of 17 mW power) were used for the samples.

SEM. The morphology of the samples was analyzed with a scanning electron microscope (Supra 55VP, SmartSEM™, Zeiss) with a field emission electron gun (FEG) using an Inlens detector and 10 kV as electron accelerating potential. For that reason, the anatase TiO<sub>2</sub> powder was dispersed in distilled water and sonicated for 5 min. 5 μL of the dispersion was dropped on a conductive carbon tape and dried. The carbon tape was fixed on an aluminium sample holder and transferred into the SEM.

XPS. X-ray photoelectron spectroscopy (XPS) analyses were carried out with an XPS spectrometer (PHI 5800, Physical Electronics) using an Al K<sub>α</sub> X-ray source. All data analysis for XPS experiments were performed and fitted with the program IGOR Pro 6.04 or CasaXPS software. The C1s peak of adventitious carbon at 284.8 eV was taken as a reference.

ICP-AES. The actual Pt loading of the samples was determined using an inductively coupled plasma atomic emission spectrometer (ICP-AES, Horiba Jobin Yvon). The powder was dissolved in aqua regia/HF using a microwave digestion system (Multiwave 3000, Anton Paar).

### **C. Photocatalytic degradation of 4-chlorophenol (4-CP)**

40 mg (0.5 mmol) of the anatase TiO<sub>2</sub>/platinized TiO<sub>2</sub> powder was dispersed in 20 mL of 2.5·10<sup>-4</sup> M 4-CP

solution and sonicated for 5 min. The suspension was irradiated for 6 h under stirring with the Ushio 150 W Xe lamp in a light-condensing lamp housing (Unnasol GmbH) with light intensity of 17 mW/cm<sup>2</sup>. Samples were taken at 0, 1, 2, 4, 6 hours. After irradiation, the samples were filtrated with a syringe filter and the electronic absorption spectra of 4-CP were measured with a Shimadzu UV-2600 UV/Vis spectrophotometer.

#### **D. Photoelectrochemical characterization**

A titanium foil (99.6+%, Advent Research Materials) was cleaned by sonication for 20 min in acetone and washed with deionized water. Then, the Ti foil was etched in a 1 vol% HF solution for 1 min and washed with deionized water. 44 mg of photocatalyst was suspended in 220  $\mu$ L ethanol and sonicated for 10 min. The suspension was smeared onto the Ti foil by the doctor blading technique using a scotch tape as frame and spacer. The electrodes were dried at RT and pressed for 3 min at a pressure of 200 kg/cm<sup>2</sup>.

All photoelectrochemical experiments were performed in a 7 mL cell in 0.1 M Na<sub>2</sub>SO<sub>4</sub> at pH 7 using the three-electrode setup with a platinum counter electrode and a Ag/AgCl (3 M KCl) reference electrode. The TiO<sub>2</sub> photoelectrodes were pressed against an O-ring of the cell, leaving an irradiated area of 0.5 cm<sup>2</sup>. The electrodes were irradiated from the front-side. The photopotential transient measurements were done under open-circuit conditions (OCP) under oxygen atmosphere (bubbling with O<sub>2</sub> for 20 min) and in an oxygen-free environment (bubbling with Ar for 30 min).

The monochromatic wavelength-resolved measurements and photocurrent onset measurements were performed using a tunable monochromatic light source (Instytut Fotonowy) provided with a 150 W xenon lamp and a grating monochromator with a bandwidth of 10 nm and an SP-300 BioLogic potentiostat. The monochromatic intensities between 320 and 800 nm were in the range of 2.8–9.7 mW/cm<sup>2</sup>. Appropriate cut-off filters were used in order to eliminate the second-order diffraction radiation. The photoaction spectra were recorded at the bias potential of 0.5 V vs Ag/AgCl in Na<sub>2</sub>SO<sub>4</sub> (0.1 M) at pH 7 under intermittent irradiation (5 s light, 5 s dark). The value of photocurrent density was taken as the difference between current density under irradiation and in the dark. The spectral dependence of lamp power density was measured by the NOVA II optical power meter equipped with a PD300-UV silicon photodiode (Ophir Optronics).

### **III. RESULTS AND DISCUSSION**

#### **A. Photodeposition of Pt on well-defined anatase TiO<sub>2</sub> crystals**

Differently sized aggregates of relatively large (~1-3  $\mu$ m) anatase TiO<sub>2</sub> crystals with well-defined facets of {101} and {001} families were prepared *via* hydrothermal synthesis using fluoride-containing solutions, as reported elsewhere.<sup>30</sup> XRD and Raman analysis confirmed the exclusive presence of anatase phase (see supplementary material, Fig. S1). The median of the relative ratio of {101} / {001} surface areas (calculated from 11 random crystals) was 0.64. Nanosized (<30 nm) Pt nanoparticles were deposited onto TiO<sub>2</sub> crystals by photoreduction of hexachloroplatinic acid in methanol-containing aqueous solutions. Interestingly, we

found deposition protocols that allow to deposit Pt nanoparticles either selectively on {101} facets (facet selective = *fs*) or non-selectively (facet non-selective = *ns*) on both {101} and {001} facets (see Figure 1). Specifically, the photoreductive deposition on *as-prepared* anatase powder resulted in *fs* deposition of Pt nanoparticles mainly on the {101} facets [Fig. 1(a)]. Similar selectivity of Pt deposition onto {101} facets has been recently reported in case of much smaller (< 100 nm) anatase nanosheets by Pellegrino *et al.*<sup>38</sup> However, if – prior to the deposition of Pt – the TiO<sub>2</sub> powder was heated at 450 °C or higher temperatures for 2 h, the deposition of Pt was not selective anymore (*ns*), resulting in Pt deposition on both {101} and {001} facets [Fig. 1(b)]. In this case, the size and overall actual loading of Pt (ca. 1 wt%) was practically the same, but the Pt nanoparticles were randomly distributed over all facets [Fig. 1(b)]. The difference between *fs* and *ns* deposition of Pt became even better apparent after Pt nanoparticles of larger size (ca. 100-150 nm) were deposited, which was achieved when the concentration of H<sub>2</sub>PtCl<sub>6</sub> precursor during photodeposition was increased by the factor of 2.25 [Fig. 1(c,d)].

The fact that on *as-prepared* TiO<sub>2</sub> crystals the Pt nanoparticles are photodeposited only on {101} facets and not on {001} facets can be best explained by the blocking effect of fluoride anions chemisorbed on {001} facets. It is known that, during hydrothermal synthesis of anatase crystals in fluoride-containing solutions, the strongly adsorbing fluoride anions exchange surface Ti–OH groups for more stable Ti–F groups,<sup>39</sup> make the {001} facets less reactive and thus effectively stabilize them during hydrothermal growth (in contrast, anatase crystals synthesized in fluoride-free solutions exhibit mostly {101} facets which are thermodynamically more stable).<sup>16,30</sup> The strongly chemisorbed fluoride anions apparently hinder the adsorption of [PtCl<sub>6</sub>]<sup>2-</sup> anions, which precludes the photoreductive deposition of Pt onto {001} facets (Figure 1a,c). Indeed, it has been reported that fluorination can hinder the adsorption of various species, such as acetaldehyde,<sup>40</sup> H<sub>2</sub>O<sub>2</sub>,<sup>41,42</sup> phenol and catechol.<sup>43,44</sup> Chloroplatinate anion itself chemisorbs onto TiO<sub>2</sub> presumably *via* formation of a covalently bound surface complex  $\{[\text{Ti}]\text{OPtCl}_4\text{L}\}^{n-}$ , where L = H<sub>2</sub>O or OH<sup>-</sup> and  $n = 1$  or  $2$ ,<sup>45</sup> and the chemisorption process should be therefore strongly hindered by fluorides. We note that an alternative explanation involving inhibition of oxidation of methanol (used as a reducing agent) at fluorinated {001} surface is less likely, since it has been reported that fluorination enhances photooxidation of methanol at TiO<sub>2</sub>.<sup>44</sup> On the other hand, when the anatase TiO<sub>2</sub> crystals were heated at 450 °C, the surface concentration of fluoride decreased from 3.4 at% to 1.2 at% as compared to non-heated material (see the corresponding XP spectra in supplementary material, Fig. S2). Herein we also note that even after a heat treatment at 600 °C for two hours, the surface fluoride was not removed completely (surface concentration ca. 1.0 at%), which is in contrast to most literature reports.<sup>16,30,31,46</sup> Hence, after the heat treatment, a substantial portion, though not all, of surface fluoride is removed, which allows for the deposition of Pt to occur now on both {101} and {001} surface facets [Fig. 1(b,d)]. In this context, we point out that this reasoning is in line with the results of Mul *et al.* on facet-selective deposition of Pt onto WO<sub>3</sub> crystals who demonstrated that the facet-specific Pt photodeposition is caused by preferential facet-specific adsorption of the Pt

precursor,<sup>47</sup> rather than by any intrinsic facet-selective separation of photogenerated charges during photodeposition. Similarly, in case of (non-fluorinated) anatase TiO<sub>2</sub>, Ohtani *et al.* recently also highlighted the importance of surface charge and adsorption properties of different facets for facet-selectivity of metal photodeposition,<sup>29</sup> and found no conclusive evidence for any intrinsic facet-selective transport of photogenerated electrons and holes to {101} and {001} facets, respectively. The latter has been frequently suggested in the literature<sup>20-27</sup> and explained, for example, by anisotropic effective mass of electrons and holes in anatase,<sup>26</sup> or by different surface energetics of {101} and {001} facets resulting in electric potential difference (band bending) at their interface.<sup>25,27,28</sup> In our case, the fact that a simple heat treatment leading to lower amount of surface fluorides can change the photodeposition from facet-specific to facet non-specific is a strong indication that the amount of surface-chemisorbed fluoride is a key factor that governs the facet specificity and non-specificity of Pt deposition at anatase crystals prepared in fluoride-containing solutions.

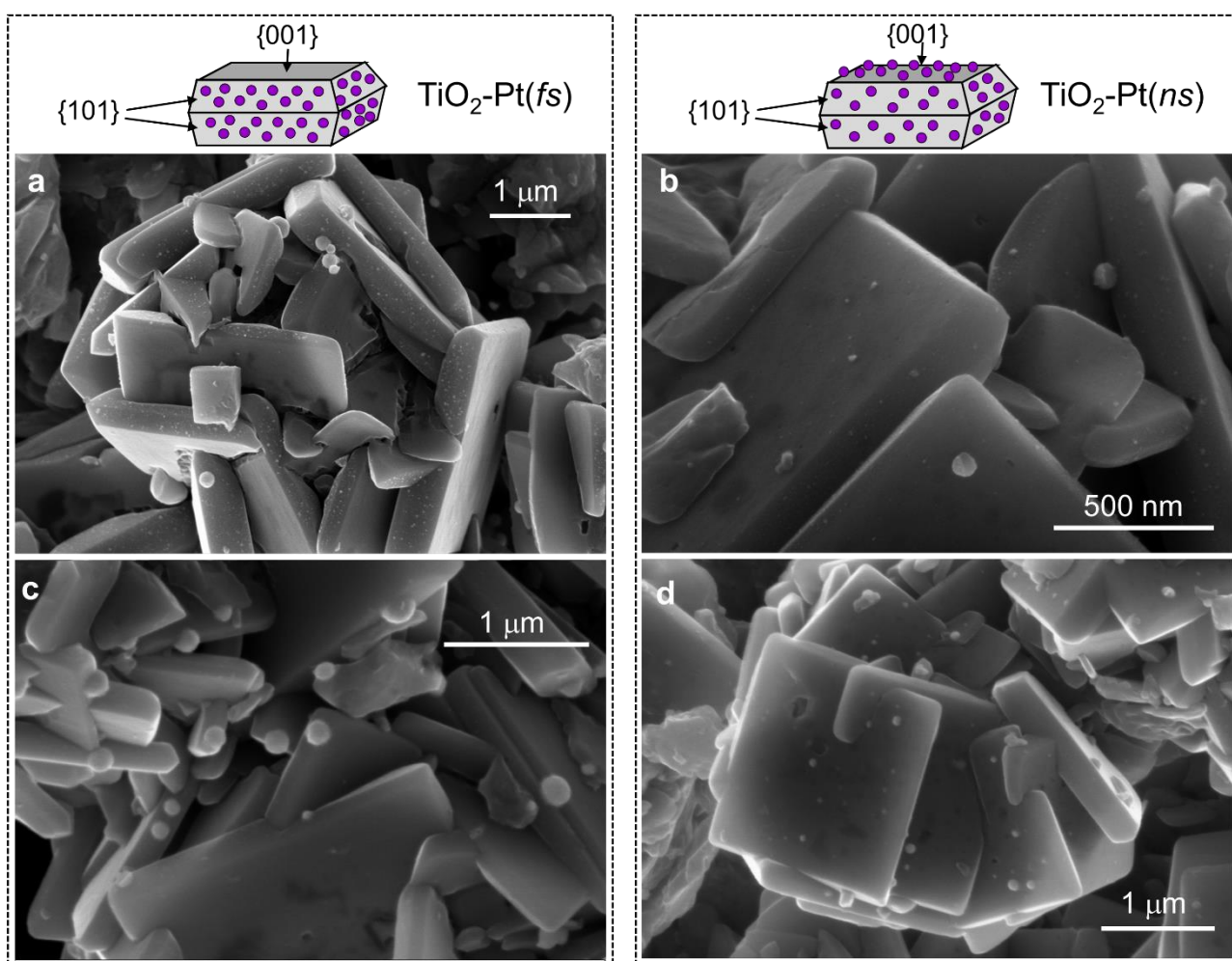


**Figure 1:** SEM images of anatase TiO<sub>2</sub> crystals with facet-selective TiO<sub>2</sub>-Pt(*fs*) (a,c) and facet non-selective TiO<sub>2</sub>-Pt(*ns*) (b,d) photodeposition of Pt nanoparticles from H<sub>2</sub>PtCl<sub>6</sub> containing solutions. Samples featuring larger (ca. 100-150 nm) Pt nanoparticles (c,d) were prepared from more concentrated H<sub>2</sub>PtCl<sub>6</sub> solutions, and exhibited lower photocatalytic activity than optimized samples with smaller (<30 nm) Pt nanoparticles (a,b).

## B. Photocatalytic properties of TiO<sub>2</sub>-Pt(*fs*) and TiO<sub>2</sub>-Pt(*ns*)

Our synthetic achievements described above allow for a comparison of photocatalytic activity of platinized TiO<sub>2</sub> crystals with facet-selectively (*fs*) and facet-non selectively (*ns*) deposited Pt nanoparticles. As a test reaction we employed photocatalytic degradation of 4-chlorophenol (4-CP), a widely used xenobiotic test pollutant of water, that also represents a useful model substance for photodegradation studies of chlorinated aromatic compounds.<sup>48</sup> Initial experiments were carried out in order to find the optimum Pt content by varying the concentration of platinum precursor solution during photodeposition, and to identify the optimum photocatalyst concentration at which the photocatalytic degradation rate was maximal. In general, we found that the photocatalytic rate was optimal for small Pt particle size (<30 nm), and decreased when the Pt particle size increased (100-150 nm). Fortunately, the optimal platinum loadings for *fs*- and *ns* platinized TiO<sub>2</sub> were very similar (0.96% and 0.92% of platinum for *fs* and *ns*, respectively, featuring particles of <30 nm size), allowing thus direct comparisons.

Figure 2(a) shows the changes of 4-CP concentration during irradiation with simulated sunlight ( $\lambda > 320$  nm) for TiO<sub>2</sub>-Pt(*fs*) and TiO<sub>2</sub>-Pt(*ns*) with optimized amounts of Pt. For direct comparison, photocatalytic degradation at non-platinized anatase TiO<sub>2</sub> crystals was investigated. Interestingly, non-platinized TiO<sub>2</sub> crystals, both heated at 450 °C and non-heated, were found to be completely *inactive* in photocatalytic degradation of 4-CP [Fig. 2(a)]. This finding cannot be readily explained solely by the effect of surface fluoride due to two reasons. Firstly, the sample after the heat treatment at 450 °C that contains much lower amount of fluoride shows negligible activity as well. Secondly, in fact, there are numerous reports on *enhancement* of photooxidation of various phenolic compounds, including 4-CP, upon surface fluorination of TiO<sub>2</sub> anatase,<sup>43,44,49,50</sup> which has been typically explained by enhanced production of OH radicals,<sup>43,51</sup> H<sub>2</sub>O<sub>2</sub>,<sup>41,42</sup> and/or lower recombination rate due to hindered adsorption of photoactivity-poisoning intermediates.<sup>44</sup> Hence, why are our non-platinized TiO<sub>2</sub> crystals completely inactive in photodegradation of 4-CP? In what follows, we propose and provide conclusive evidence for a hypothesis that the key factor influencing the rate of 4-CP degradation in our case is the rate of oxygen reduction by photogenerated electrons. The crucial role of oxygen reduction in photocatalytic degradation has been suggested already by Gerischer and Heller in the 1990's,<sup>35,52</sup> and later confirmed by transient absorption spectroscopy studies which have demonstrated that the reduction of dioxygen by photogenerated electrons occurs much slower (by ca. three orders of magnitude) than oxidation of organics (such as alcohols) by photogenerated holes.<sup>53,54</sup> Moreover, Gerischer and Heller also argued, based on a theoretical analysis, that the effect of oxygen reduction rate on quantum efficiency should become much more severe when the TiO<sub>2</sub> photocatalytic particle size exceeds 1  $\mu$ m and the surface-to-volume ratio of the particles decreases dramatically, in contrast to a relatively large specific surface area of typical photocatalytic powders featuring crystallites of 5-

100 nm size. Since the oxygen reduction can occur only on the photocatalyst surface, the overall lower rate of electron consumption, as compared to electron-hole pair generation rate, will inevitably lead to accumulation of electrons in the photocatalyst particles. This, in turn, will translate into almost complete recombination.<sup>52</sup> In our case the particle size is ca. 1–3  $\mu\text{m}$ , hence one can assume that the oxygen reduction rate is the main limiting factor in photocatalytic degradation. Moreover, the effect is most likely amplified by surface fluorination, which is known to lower the reactivity of photogenerated electrons towards electron acceptors, including dissolved oxygen, at  $\text{TiO}_2$  surfaces,<sup>44,55</sup> which has been explained by high electronegativity of fluorine atoms that contributes to stabilization of electrons trapped at surface Ti-F sites.<sup>43,51</sup>

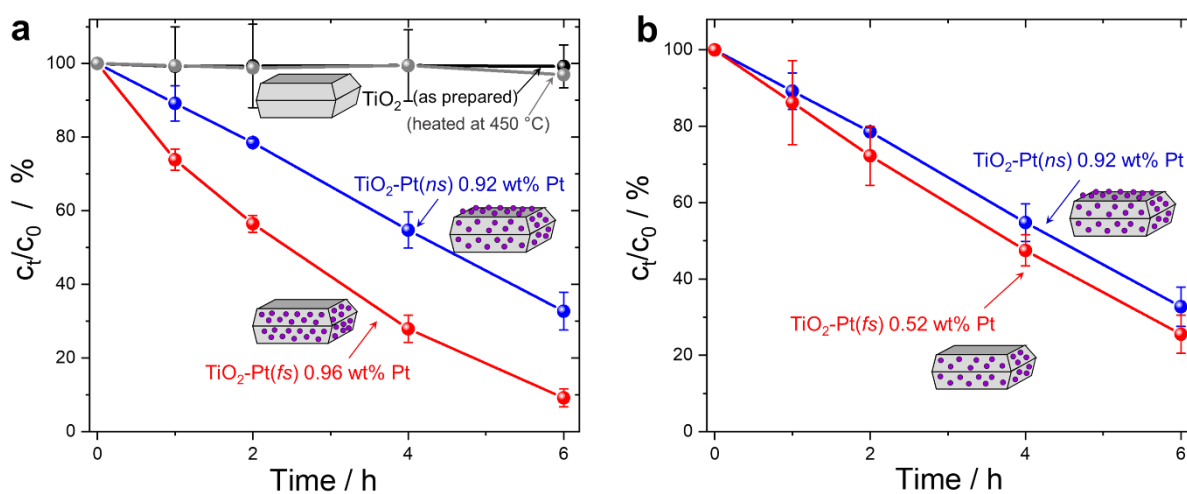


**Figure 1:** Changes of 4-CP concentration in aqueous suspensions of various samples during photocatalytic degradation experiments performed under simulated sunlight irradiation ( $\lambda > 320$  nm; intensity  $\sim 17$  mW/cm<sup>2</sup>): (a) comparison of pristine  $\text{TiO}_2$  anatase crystals (as-prepared and heated at 450 °C for 2 hours) with platinized  $\text{TiO}_2$  with facet-specific [ $\text{TiO}_2\text{-Pt}(fs)$ ] and facet non-specific [ $\text{TiO}_2\text{-Pt}(ns)$ ] deposition. (b) Comparison of photocatalytic performance of  $\text{TiO}_2\text{-Pt}(fs)$  and  $\text{TiO}_2\text{-Pt}(ns)$  with different Pt loadings.

However, already in the seminal paper by Gerischer and Heller,<sup>52</sup> it has been proposed that the limitations related to low oxygen reduction rate can be overcome by use of cocatalysts for oxygen reduction. Indeed, this is exactly what we observe after deposition of Pt nanoparticles, a prototypical catalyst for oxygen reduction.<sup>34,35,37,56</sup> The deposition of Pt effectively triggers the photocatalytic degradation of 4-CP [Fig. 2(a)]. Two further important facts are noteworthy. Firstly, at the same overall Pt loading of ca. 1 wt%, the  $\text{TiO}_2\text{-Pt}(fs)$  material clearly outperforms  $\text{TiO}_2\text{-Pt}(ns)$ , as the initial degradation rate (after 1 hour) is more than twice as high for  $\text{TiO}_2\text{-Pt}(fs)$  that has Pt nanoparticles only on the {101} facets. Secondly, when the Pt deposition is facet-selective on {101} facets, one can achieve the same degradation rate with approximately half amount (56%) of Pt as compared to the case of

non-selective deposition [Fig. 2(b)]. These observations clearly suggest that only Pt nanoparticles deposited on {101} facets do effectively enhance photocatalysis, whereby the enhancement effect of Pt nanoparticles deposited on {001} is negligible. This is a significant finding since it highlights the beneficial effect of facet-selective deposition of Pt that can be leveraged for a more economic way of utilization of noble metal catalysts, such as Pt, in photocatalysis. However, a question arises as to *why* exactly, at both TiO<sub>2</sub>-Pt(*fs*) and TiO<sub>2</sub>-Pt(*ns*), *only Pt deposited on {101} facets enhances photocatalysis*? Based on the fact that photoreductive deposition of Pt is clearly at work also on {001} facets at heated TiO<sub>2</sub> crystals, we rule out the possibility that the above effect is caused primarily by an inherently anisotropic charge transport in our crystals that would drive photogenerated electrons preferentially to {101} facets and holes to {001} facets, as often invoked in the literature.<sup>20-27</sup> A much more plausible explanation is that the {001} facets are, even after deposition of Pt nanoparticles, to a large extent *inactive* in photooxidation of 4-CP. Indeed, this explanation is in line with a number of reports on inhibited photocatalytic activity of TiO<sub>2</sub> anatase crystals with mainly exposed {001} facets,<sup>21,30,46,57</sup> whereby in all these cases the crystals were previously subjected to a heat treatment in order to remove surface fluorides. Importantly, Mino et al. recently proposed that the main reason for the inactivity of {001} facets in such cases might be the (1 × 4) reconstruction of the {001} facets upon the heat treatment.<sup>46</sup> Such stress-driven (1 × 4) reconstruction at (001) anatase surfaces<sup>58</sup> is experimentally well established,<sup>59-61</sup> and has been theoretically predicted to lead to a loss of reactivity with respect to the dissociative adsorption of water.<sup>62,63</sup> Indeed, Mino *et al.* found that, as a consequence, the reconstructed {001} facets exhibit a lower degree of hydroxylation, lower hydrophilicity and weaker Lewis acidity of Ti(IV) sites, whereby all these aspects exert a negative effect on the reactivity of reconstructed {001} surfaces in photooxidation of phenolic compounds.<sup>46,64</sup> In other words, even if we assumed that oxygen can be possibly reduced by photogenerated electrons at Pt deposited on {001} facets, 4-CP molecules would not be available at {001} facets for reaction with oxidative equivalents (holes or reactive radicals), which would result in recombination. In contrast, {101} facets apparently possess active sites for 4-CP oxidation, which allows for degradation of 4-CP upon activation of oxygen at Pt nanoparticles at {101} facets. The detrimental effects associated with the (1 × 4) reconstruction at {001} facets are thus the most likely explanation for the inactivity of {001} facets in 4-CP photodegradation. At the same time, this explanation sheds also light on other reports of very low photocatalytic activity of anatase crystals dominated by {001} facets, both in form of large (>2 μm)<sup>21,30</sup> and small (<100 nm)<sup>46,57</sup> crystals.

### C. Mechanistic studies

So far, we have established that photocatalysis is, in our case, triggered by Pt nanoparticles deposited on {101} facets. As a next step we performed a series of experiments to prove that this triggering effect

can be ascribed chiefly to enhanced oxygen reduction by photogenerated electrons through effective catalysis at Pt nanoparticles. Firstly, control experiments performed either in the dark, or under irradiation but in the absence of oxygen, showed no degradation of 4-CP (see supplementary material, Fig. S3). This clearly shows that the process is photocatalytic and that oxygen is the only effective oxidizing agent. Hence, the anoxic degradation of organic pollutants concomitant with H<sub>2</sub> production that has been reported in the literature can be ruled out in our case.<sup>65,66</sup>

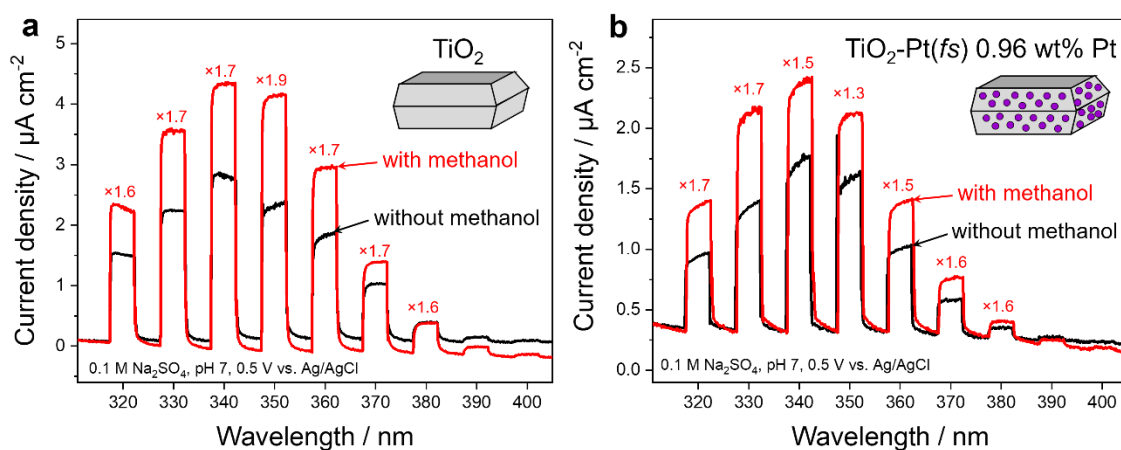


**Figure 3:** Photocurrents measured under intermittent monochromatic irradiation at different wavelengths (5 s light, 5 s dark) for  $\text{TiO}_2$  (a) and  $\text{TiO}_2\text{-Pt}(fs)$  (b) samples deposited onto Ti foils in 0.1 M  $\text{Na}_2\text{SO}_4$  (pH 7) at a constant potential of 0.5 V vs. Ag/AgCl. The experiments were carried out either without or with addition of methanol as additional reducing agent; the numbers above transients indicate the relative enhancement of photocurrent upon addition of methanol.

Secondly, since platinum is known to act as an excellent hydrogen transfer catalyst, it could be possible that also the oxidative pathway, initiated by photogenerated holes, is enhanced by deposition of Pt nanoparticles. In order to test this possibility, we carried out a series of photocurrent measurements with pristine  $\text{TiO}_2$  and  $\text{TiO}_2\text{-Pt}(fs)$  crystals deposited onto titanium foil in the presence and in the absence of methanol. Figure 3 shows that, as expected, the photocurrents increase with addition of methanol since methanol is a more readily oxidizable reducing agent than water. However, the relative enhancement of photocurrent upon addition of methanol is practically the same for both  $\text{TiO}_2$  and  $\text{TiO}_2\text{-Pt}(fs)$ . This means that the deposition of Pt does not, *per se*, enhance the oxidative kinetics, and its triggering effect on photocatalysis can be ascribed to the enhancement of the reductive pathway, *i.e.*, to improved reduction of oxygen.

Thirdly, in order to account more quantitatively for the differences in reaction kinetics of

photogenerated electrons with oxygen in the presence and absence of Pt catalyst, we deposited both pristine TiO<sub>2</sub> and TiO<sub>2</sub>-Pt(*fs*) crystals onto Ti foils, and investigated the kinetics of the open-circuit photopotential decay after switching off the light.<sup>38,55,67,68</sup> As usual, TiO<sub>2</sub>-based photoelectrodes show negative photopotentials since, during irradiation, photogenerated electrons accumulate in TiO<sub>2</sub> and are transported to the underlying electrode, shifting thus its Fermi level to more negative electrode potentials (supplementary material, Fig. S4). After switching-off the light, the photopotential decays due to both recombination and interfacial electron transfer to species in the electrolyte. The differences in kinetics related distinctly to the differences in the rate of reaction with oxygen are thus accessible when decay kinetics are compared between measurements done in the absence and in the presence of dissolved oxygen. In order to account at least semi-quantitatively for the different reaction rates with oxygen at TiO<sub>2</sub> crystals without and with Pt nanoparticles, we derive the momentous electron lifetime in dependence on the momentous photopotential, following the simplified formalism of Zaban *et al.*<sup>69</sup> Assuming the first-order kinetics of global electron consumption (by both recombination and electron transfer) with respect to the concentration of electrons ( $n$ ) in TiO<sub>2</sub>, the electron lifetime  $\tau$  can be defined as  $\tau = -\frac{1}{n} \frac{dn}{dt}$  (1). The measured photopotential  $V_{ph}$  is defined as the difference in open-circuit potential under illumination and in the dark,  $V_{ph} = V_{oc}^{light} - V_{oc}^{dark}$ . Using the Boltzmannian approximation of the Fermi-Dirac distribution function (*i.e.*, assuming  $*E_{Fn} - E_c \gg kT$ , where  $E_c$  is the energy of the conduction band edge and  $*E_{Fn}$  is the *quasi*-Fermi level of electrons),  $V_{ph}$  can be expressed as  $V_{ph} = -\frac{kT}{e} \ln\left(\frac{n}{n_0}\right)$  (2), where  $e$  is the (positive) elementary charge,  $k$  is the Boltzmann constant,  $T$  is the absolute temperature, and  $n_0$  is the concentration of electrons in the dark. Combining equations (1) and (2), one obtains for the electron lifetime the relation:  $\tau = \frac{kT}{e} \left(\frac{dV_{ph}}{dt}\right)^{-1}$  (3).

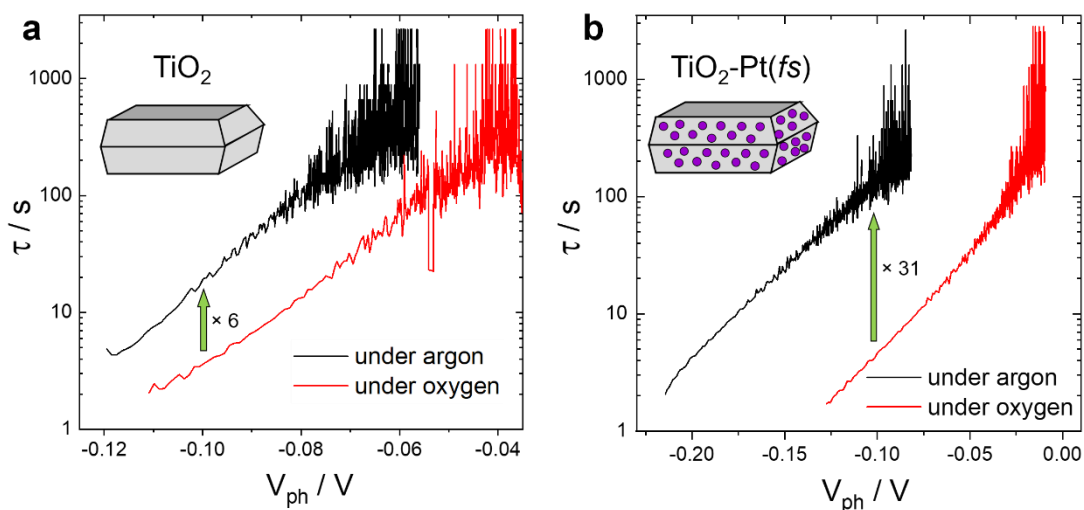


**Figure 2:** The electron lifetime  $\tau$  as a function of photopotential  $V_{ph}$  for  $\text{TiO}_2$  (a) and  $\text{TiO}_2\text{-Pt}(fs)$  crystals (b) derived from photopotential decay transients after switching-off the light (using Equation 3). The numbers next to the arrows indicate the relative decrease of electron lifetime in the presence of oxygen *versus* without oxygen. The data shown were derived from the second transient decay (see the supplementary material, Fig. S4); the lifetime trends were practically the same for all transients.

Figure 4 shows that, as expected, at both  $\text{TiO}_2$  and  $\text{TiO}_2\text{-Pt}(fs)$ , the electron lifetimes are, at all photopotentials, systematically lower in oxygen-containing solutions than in the absence of oxygen, since an additional electron consumption pathway, apart from recombination, is made available. Most importantly, while at pristine  $\text{TiO}_2$  crystals the electron lifetime is shorter by the factor of 6 [Fig. 4(a)], at  $\text{TiO}_2\text{-Pt}(fs)$  the presence of oxygen shortens the electron lifetime even by the factor of 31 [Fig. 4(b)]. This suggests that the overall kinetics of oxygen reduction is enhanced by the factor of  $\sim 5$  upon Pt deposition. In this context, we also point out that we found no evidence for any significant band bending in  $\text{TiO}_2$  crystals upon deposition of Pt nanoparticles, since the deposition of Pt did not induce any shift of Ti 2p core level binding energies in XP spectra (see supplementary material, Fig. S5). Our results thus clearly show that the triggering effect of Pt deposition on photocatalytic degradation of 4-CP [Fig. 2(a)] is based chiefly on catalytically enhanced reduction of oxygen by photogenerated electrons at Pt nanoparticles deposited on {101} facets, which effectively channels photogenerated electrons out of  $\text{TiO}_2$  crystals and diminishes thus their recombination with holes.

#### IV. CONCLUSIONS

Our study addresses several important aspects of photocatalysis at well-defined anatase  $\text{TiO}_2$  crystals, and, based on that, provides also a good platform for a more general reconsideration of factors

governing the charge separation and photoconversion efficiencies in photocatalysis with particulate semiconductors. Firstly, we present protocols that enable the photoreductive deposition of Pt nanoparticles onto well-defined anatase TiO<sub>2</sub> crystals prepared by hydrothermal growth in fluoride-containing solutions to be carried out either facet-selectively (on {101} facets only) or facet non-selectively (on both {101} and {001} facets). The key factor influencing the selectivity is the amount of fluoride anions strongly chemisorbed on {001} facet surfaces. At higher surface concentration of fluorides, the deposition of Pt at {001} facets is hindered, and Pt deposits only at {101} facets. Upon decreasing the concentration of surface fluorides by a heat treatment, the Pt deposition occurs also on {001} facets. Secondly, we demonstrate that the deposition of Pt nanoparticles effectively triggers the photocatalytic degradation of 4-CP at anatase crystals which were, without Pt, photocatalytically completely inactive. Thirdly, we show that the triggering effect of Pt consists in catalytic enhancement of the reaction rate of oxygen reduction by photogenerated electrons, which is known to play a key role in photocatalytic degradation of organic compounds,<sup>34,35,37,56,67,68,70-72</sup> especially when TiO<sub>2</sub> particles are relatively large (size > 1 μm).<sup>52</sup> Finally, we found that only platinized {101} facets contribute to photocatalysis. In contrast, the {001} facets, in the literature often referred to as “highly reactive”,<sup>16-19</sup> are even after platinization completely inactive, most likely due to (1 × 4) surface reconstruction upon the heat treatment and concomitant change in adsorption and catalytic properties of the interface that exert a negative influence on reactivity of 4-CP.<sup>46,64</sup>

Our results highlight the eminent role of proper interfacial engineering and surface chemistry for photocatalytic activity. In our case, the surface adsorption and redox catalytic properties of the interface are demonstrated to completely control whether photocatalysis is at work or not. Furthermore, the fact that {001} facets after (1 × 4) surface reconstruction are completely inactive even in the presence of a catalyst very well exemplifies how even minute changes in surface structure may drastically influence photocatalytic activity. In this context, we point out at a recent report by Macyk *et al.* who showed how the photoactivity of TiO<sub>2</sub> powder photocatalysts may change significantly upon supposedly insignificant modifications of surface structure, such as deposition of tiny amounts of TiO<sub>2</sub> by few cycles of atomic layer deposition (ALD).<sup>73</sup> Therefore, we envisage that “gentle” surface modification methods like ALD may be leveraged for interfacial engineering of, for example, {001} facets on atomic level with high impact on photocatalytic activity. Importantly, in line with results of Mul *et al.*<sup>47</sup> and Ohtani *et al.*,<sup>29</sup> we found no evidence for inherently anisotropic charge transport in crystals with well-defined facets that would, rather independently from reactions occurring at the surface, drive photogenerated electrons preferentially to {101} facets and holes to {001} facets, as often suggested.<sup>20-27</sup> *Is then the proposal to utilize well-defined crystals for construction of highly efficient photocatalysts with oxidation and reduction reactions occurring at different facets simply misguided?* No, but we would argue that the conventional picture of anisotropic charge transport in

such systems based solely on *intrinsic* properties, such as anisotropic effective mass of electrons and holes in anatase<sup>26</sup> or “surface heterojunction” at the interface of {101} and {001} facets, mostly derived from theoretical calculations or surface energetics determined by spectroscopy under UHV conditions,<sup>25,27,28</sup> is—at best—incomplete, and—at worst—misleading, as documented by controversies regarding the photocatalytic activity of well-defined TiO<sub>2</sub> crystals with large amount of {001} facets.<sup>18,19,21,30,31</sup> Indeed, it is possibly the very key aspect that is missing in such a picture, namely the *redox catalytic* properties of specific interfaces towards specific desired redox reactions, *i.e.*, the specific surface chemistry and its kinetics, which should ensure that photogenerated electrons and holes are consumed in redox reactions before they recombine. Indeed, the key role of surface chemistry in photocatalysis has been recently highlighted by Heiz *et al.*,<sup>74</sup> and can be also well-exemplified by recent theoretical work of Selcuk and Selloni that suggests that, for example, the photogenerated electron trapping properties of different facets of anatase TiO<sub>2</sub> depend strongly on the environment and the nature of the electron donor.<sup>75</sup>

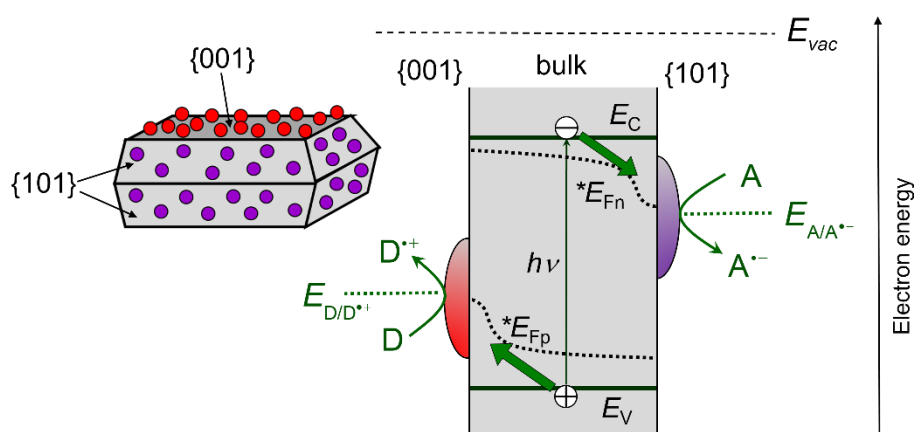


**Figure 5:** A proposed design scenario and an energy scheme for a highly efficient photocatalytic system comprising two different catalysts for specific oxidation and reduction reactions selectively deposited at distinct crystal facets of the photocatalyst. Efficient redox catalysis of interfacial redox reactions, reduction of electron acceptor A by photogenerated electrons and oxidation of electron donor D by photogenerated holes, is the key prerequisite for avoiding the recombination and maximizing thus the quantum efficiency.  $E_c$  and  $E_v$  is the energy of the conduction and valence band edge, respectively.  $*E_{Fn}$  and  $*E_{Fp}$  denote the *quasi*-Fermi levels (corresponding to electrochemical potentials,  $*E_{Fn} = \tilde{\mu}_n$  and  $*E_{Fp} = -\tilde{\mu}_p$ ) of electrons and holes, respectively.  $E_{A/A^{*-}}$  and  $E_{D/D^{*+}}$  stand for redox Fermi levels of electron acceptor A and electron donor D in solution, respectively. Note that, in this example, the local vacuum level ( $E_{vac}$ ) is depicted as a straight line in order to highlight the fact that there is no need for a gradient of *electric* potential within the photocatalytic system; the charge separation occurs primarily *kinetically*, as the driving force is the gradient of *electrochemical* potentials of electrons and holes provided by *fast* catalytic redox reactions at the interfaces.

In this context, we recall the seminal contribution by Peter Würfel on the nature of charge separation in solar energy-converting devices.<sup>76</sup> In any photoconversion system, be it a silicon solar cell or a TiO<sub>2</sub> photocatalyst, efficient charge separation (understood as the opposite of recombination) occurs, in principle, due to the gradient of *quasi*-Fermi levels (*i.e.*, of electrochemical potential) of electrons and holes at well-designed and spatially separated interfaces that act as selective (semi-permeable) membranes, letting through only either electrons or holes. Our study suggests that, in photocatalysis, it is primarily the efficient redox catalysis that makes a specific interface an effective selective membrane, and creates thus the necessary gradient of electrochemical potentials of electrons and holes by modifying mainly their chemical (*i.e.*, concentration) parts (Fig.5). In other words, in case of TiO<sub>2</sub> photocatalytic degradation of organic compounds, any design of proper function of various crystal facets as selective membranes for either electrons or holes should include facet-specific deposition of catalysts for reduction of dioxygen and oxidation of organic compounds. In a similar vein to recent efforts to enhance photocatalysis at BiVO<sub>4</sub> crystals,<sup>77</sup> the different, and possibly tuneable, reactivity of {101} and {001} facets at anatase TiO<sub>2</sub> crystals may open the route for fabrication of precisely such well-designed photocatalytic “micro-solar cell” architectures with unprecedented quantum efficiencies.

#### **SUPPLEMENTARY MATERIAL**

See the supplementary material for blank degradation experiments and for additional XPS, Raman, XRD, and photopotential transients data.

#### **ACKNOWLEDGEMENTS**

The Deutsche Forschungsgemeinschaft (DFG) is gratefully acknowledged for financial support (BE 5102/5-1 and 364549901, TRR 234 “Catalight” [Project B6]). I.K. acknowledges the support of the Alexander von Humboldt Foundation through the Humboldt Research Fellowship. We thank Dr. Thomas Diemant for XPS measurements, and Margit Lang for ICP-AES analyses.

**The data that support the findings of this study are available from the corresponding author upon reasonable request.**

#### **REFERENCES**

- <sup>1</sup> M. R. Hoffmann, S. T. Martin, W. Choi, and D. W. Bahnemann, *Chem. Rev.* **95**, 69 (1995).
- <sup>2</sup> X. Chen, S. Shen, L. Guo, and S. S. Mao, *Chem. Rev.* **110**, 6503 (2010).
- <sup>3</sup> B. Ohtani, *J. Photochem. Photobiol. C* **11**, 157 (2010).
- <sup>4</sup> H. Kisch, *Angew. Chem., Int. Ed.* **52**, 812 (2013).

- <sup>5</sup> H. Kisch, *Semiconductor Photocatalysis: Principles and Applications* (Wiley-VCH, Weinheim, 2015).
- <sup>6</sup> J. Z. Bloh, and R. Marschall, *Eur. J. Org. Chem.* **2017**, 2085 (2017).
- <sup>7</sup> R. Beranek, *Angew. Chem., Int. Ed.* **58**, 16724 (2019).
- <sup>8</sup> I. Krivtsov, D. Mitoraj, C. Adler, M. Ilkaeva, M. Sardo, L. Mafra, C. Neumann, A. Turchanin, C. Li, B. Dietzek, R. Leiter, J. Biskupek, U. Kaiser, C. Im, B. Kirchhoff, T. Jacob, and R. Beranek, *Angew. Chem., Int. Ed.* **59**, 487 (2020).
- <sup>9</sup> O. Carp, C. L. Huisman, and A. Reller, *Prog. Solid State Chem.* **32**, 33 (2004).
- <sup>10</sup> M. A. Henderson, *Surf. Sci. Rep.* **66**, 185 (2011).
- <sup>11</sup> M. Addamo, V. Augugliaro, A. Di Paola, E. Garcia-Lopez, V. Loddo, G. Marci, R. Molinari, L. Palmisano, and M. Schiavello, *J. Phys. Chem. B* **108**, 3303 (2004).
- <sup>12</sup> M. Xu, Y. Gao, E. M. Moreno, M. Kunst, M. Muhler, Y. Wang, H. Idriss, and C. Woll, *Phys. Rev. Lett.* **106**, 138302 (2011).
- <sup>13</sup> M. Buchalska, M. Kobielski, A. Matuszek, M. Pacia, S. Wojtyła, and W. Macyk, *ACS Catal.* **5**, 7424 (2015).
- <sup>14</sup> L. Sun, and J. Bolton, *J. Phys. Chem.* **100**, 4127 (1996).
- <sup>15</sup> A. Emeline, A. Salinaro, and N. Serpone, *J. Phys. Chem. B* **104**, 11202 (2000).
- <sup>16</sup> H. G. Yang, C. H. Sun, S. Z. Qiao, J. Zou, G. Liu, S. C. Smith, H. M. Cheng, and G. Q. Lu, *Nature* **453**, 638 (2008).
- <sup>17</sup> X.-Q. Gong, and A. Selloni, *J. Phys. Chem. B* **109**, 19560 (2005).
- <sup>18</sup> X. Han, Q. Kuang, M. Jin, Z. Xie, and L. Zheng, *J. Am. Chem. Soc.* **131**, 3152 (2009).
- <sup>19</sup> W. Q. Fang, X.-Q. Gong, and H. G. Yang, *J. Phys. Chem. Lett.* **2**, 725 (2011).
- <sup>20</sup> T. Ohno, K. Sarukawa, and M. Matsumura, *New J. Chem.* **26**, 1167 (2002).
- <sup>21</sup> T. Tachikawa, S. Yamashita, and T. Majima, *J. Am. Chem. Soc.* **133**, 7197 (2011).
- <sup>22</sup> Z. Zheng, B. Huang, J. Lu, X. Qin, X. Zhang, and Y. Dai, *Chem. Eur. J.* **17**, 15032 (2011).
- <sup>23</sup> C. Liu, X. Han, S. Xie, Q. Kuang, X. Wang, M. Jin, Z. Xie, and L. Zheng, *Chemistry – An Asian Journal* **8**, 282 (2013).
- <sup>24</sup> X. Wang, T. Li, R. Yu, H. Yu, and J. Yu, *J. Mater. Chem. A* **4**, 8682 (2016).
- <sup>25</sup> J. Yu, J. Low, W. Xiao, P. Zhou, and M. Jaroniec, *J. Am. Chem. Soc.* **136**, 8839 (2014).
- <sup>26</sup> M. Kus, T. Altantzis, S. Vercauteren, I. Caretti, O. Leenaerts, K. J. Batenburg, M. Mertens, V. Meynen, B. Partoens, S. Van Doorslaer, S. Bals, and P. Cool, *J. Phys. Chem. C* **121**, 26275 (2017).
- <sup>27</sup> S. Kashiwaya, T. Toupance, A. Klein, and W. Jaegermann, *Adv. Energy Mater.* **8**, 1802195 (2018).
- <sup>28</sup> G. Di Liberto, S. Tosoni, and G. Pacchioni, *J. Phys. Chem. Lett.* **10**, 2372 (2019).
- <sup>29</sup> K. Kobayashi, M. Takashima, M. Takase, and B. Ohtani, *Catalysts* **8**, 542 (2018).
- <sup>30</sup> J. Pan, G. Liu, G. Q. Lu, and H.-M. Cheng, *Angew. Chem., Int. Ed.* **50**, 2133 (2011).
- <sup>31</sup> M. Maisano, M. V. Dozzi, M. Coduri, L. Artiglia, G. Granozzi, and E. Selli, *ACS Appl. Mater. Interfaces* **8**, 9745 (2016).
- <sup>32</sup> B. Kraeutler, and A. J. Bard, *J. Am. Chem. Soc.* **100**, 4317 (1978).
- <sup>33</sup> A. Mills, *J. Chem. Soc., Chem. Commun.*, 367 (1982).
- <sup>34</sup> D. W. Bahnemann, J. Mönig, and R. Chapman, *J. Phys. Chem.* **91**, 3782 (1987).

- <sup>35</sup> H. Gerischer, and A. Heller, *J. Phys. Chem.* **95**, 5261 (1991).
- <sup>36</sup> B. Ohtani, K. Iwai, S.-i. Nishimoto, and S. Sato, *J. Phys. Chem. B* **101**, 3349 (1997).
- <sup>37</sup> D. Hufschmidt, D. Bahnemann, J. J. Testa, C. A. Emilio, and M. I. Litter, *J. Photochem. Photobiol. A* **148**, 223 (2002).
- <sup>38</sup> F. Pellegrino, F. Sordello, L. Mino, C. Minero, V.-D. Hodoroaba, G. Martra, and V. Maurino, *ACS Catal.* **9**, 6692 (2019).
- <sup>39</sup> M. Herrmann, U. Kaluza, and H. P. Boehm, *Zeitschrift für anorganische und allgemeine Chemie* **372**, 308 (1970).
- <sup>40</sup> H. Kim, and W. Choi, *Appl. Catal. B: Environ.* **69**, 127 (2007).
- <sup>41</sup> V. Maurino, C. Minero, G. Mariella, and E. Pelizzetti, *Chem. Commun.*, 2627 (2005).
- <sup>42</sup> M. Mrowetz, and E. Selli, *New J. Chem.* **30**, 108 (2006).
- <sup>43</sup> H. Park, and W. Choi, *J. Phys. Chem. B* **108**, 4086 (2004).
- <sup>44</sup> D. Monllor-Satoca, T. Lana-Villarreal, and R. Gómez, *Langmuir* **27**, 15312 (2011).
- <sup>45</sup> G. Burgeth, and H. Kisch, *Coord. Chem. Rev.* **230**, 41 (2002).
- <sup>46</sup> L. Mino, F. Pellegrino, S. Rades, J. Radnik, V.-D. Hodoroaba, G. Spoto, V. Maurino, and G. Martra, *ACS Applied Nano Materials* **1**, 5355 (2018).
- <sup>47</sup> K. Wenderich, A. Klaassen, I. Siretanu, F. Mugele, and G. Mul, *Angew. Chem., Int. Ed.* **53**, 12476 (2014).
- <sup>48</sup> J. Theurich, M. Lindner, and D. W. Bahnemann, *Langmuir* **12**, 6368 (1996).
- <sup>49</sup> S. Kim, and W. Choi, *J. Phys. Chem. B* **109**, 5143 (2005).
- <sup>50</sup> S. Cong, and Y. Xu, *J. Hazard. Mater.* **192**, 485 (2011).
- <sup>51</sup> M. Mrowetz, and E. Selli, *Phys. Chem. Chem. Phys.* **7**, 1100 (2005).
- <sup>52</sup> H. Gerischer, and A. Heller, *J. Electrochem. Soc.* **139**, 113 (1992).
- <sup>53</sup> Y. Tamaki, A. Furube, M. Murai, K. Hara, R. Katoh, and M. Tachiya, *J. Am. Chem. Soc.* **128**, 416 (2006).
- <sup>54</sup> L. Jing, Y. Cao, H. Cui, J. R. Durrant, J. Tang, D. Liu, and H. Fu, *Chem. Commun.* **48**, 10775 (2012).
- <sup>55</sup> D. Monllor-Satoca, and R. Gomez, *J. Phys. Chem. C* **112**, 139 (2008).
- <sup>56</sup> A. A. Ismail, and D. W. Bahnemann, *J. Phys. Chem. C* **115**, 5784 (2011).
- <sup>57</sup> F. Pellegrino, E. Morra, L. Mino, G. Martra, M. Chiesa, and V. Maurino, *J. Phys. Chem. C* **124**, 3141 (2020).
- <sup>58</sup> M. Lazzeri, and A. Selloni, *Phys. Rev. Lett.* **87**, 266105 (2001).
- <sup>59</sup> K. Fang, G. Li, Y. Ou, W. Yuan, H. Yang, Z. Zhang, and Y. Wang, *J. Phys. Chem. C* **123**, 21522 (2019).
- <sup>60</sup> W. Yuan, Y. Wang, H. Li, H. Wu, Z. Zhang, A. Selloni, and C. Sun, *Nano Lett.* **16**, 132 (2016).
- <sup>61</sup> W. Yuan, H. Wu, H. Li, Z. Dai, Z. Zhang, C. Sun, and Y. Wang, *Chem. Mater.* **29**, 3189 (2017).
- <sup>62</sup> S. Selçuk, and A. Selloni, *J. Phys. Chem. C* **117**, 6358 (2013).
- <sup>63</sup> E. Vitale, G. Zollo, L. Agosta, F. Gala, E. G. Brandt, and A. Lyubartsev, *J. Phys. Chem. C* **122**, 22407 (2018).
- <sup>64</sup> L. Mino, C. Negri, A. Zecchina, and G. Spoto, **230**, 1441 (2016).
- <sup>65</sup> J. Kim, J. Lee, and W. Choi, *Chem. Commun.*, 756 (2008).

- <sup>66</sup> J. Kim, D. Monllor-Satoca, and W. Choi, *Energy Environ. Sci.* **5**, 7647 (2012).
- <sup>67</sup> S. Neubert, P. Pulisova, C. Wiktor, P. Weide, B. Mei, D. A. Guschin, R. A. Fischer, M. Muhler, and R. Beranek, *Catal. Today* **230**, 97 (2014).
- <sup>68</sup> S. Neubert, D. Mitoraj, S. A. Shevlin, P. Pulisova, M. Heimann, Y. Du, G. K. L. Goh, M. Pacia, K. Kruczala, S. Turner, W. Macyk, Z. X. Guo, R. K. Hocking, and R. Beranek, *J. Mater. Chem. A* **4**, 3127 (2016).
- <sup>69</sup> A. Zaban, M. Greenshtein, and J. Bisquert, *ChemPhysChem* **4**, 859 (2003).
- <sup>70</sup> J. Patzsch, and J. Z. Bloh, *Catal. Today* **300**, 2 (2018).
- <sup>71</sup> J. Patzsch, Jacob N. Spencer, A. Folli, and J. Z. Bloh, *RSC Advances* **8**, 27674 (2018).
- <sup>72</sup> S. Kohsakowski, P. Pulisova, D. Mitoraj, S. Neubert, J. Biskupek, U. Kaiser, S. Reichenberger, G. Marzun, and R. Beranek, *Small Methods* **3**, 1800390 (2019).
- <sup>73</sup> M. Trochowski, M. Kobielski, K. Mróz, M. Surówka, J. Hämäläinen, T. Iivonen, M. Leskelä, and W. Macyk, *J. Mater. Chem. A* **7**, 25142 (2019).
- <sup>74</sup> C. A. Walenta, M. Tschurl, and U. Heiz, *J. Phys.: Condens. Matter* **31**, 473002 (2019).
- <sup>75</sup> S. Selcuk, and A. Selloni, *Nat. Mater.* **15**, 1107 (2016).
- <sup>76</sup> P. Würfel, *Physics of Solar Cells: From Principles to New Concepts* (Wiley-VCH, Weinheim, 2005).
- <sup>77</sup> R. Li, F. Zhang, D. Wang, J. Yang, M. Li, J. Zhu, X. Zhou, H. Han, and C. Li, *Nat Commun* **4**, 1432 (2013).

# On the importance of catalysis in photocatalysis: Triggering of photocatalysis at well-defined anatase TiO<sub>2</sub> crystals through facet-specific deposition of oxygen reduction cocatalyst

Christiane Adler,<sup>a</sup> Dariusz Mitoraj,<sup>a</sup> Igor Krivtsov,<sup>a</sup> Radim Beranek<sup>a\*</sup>

<sup>a</sup> Institute of Electrochemistry, Ulm University, Albert-Einstein-Allee 47, 89081, Ulm, Germany

\* Corresponding author: E-mail: [radim.beranek@uni-ulm.de](mailto:radim.beranek@uni-ulm.de)

## SUPPLEMENTARY MATERIAL

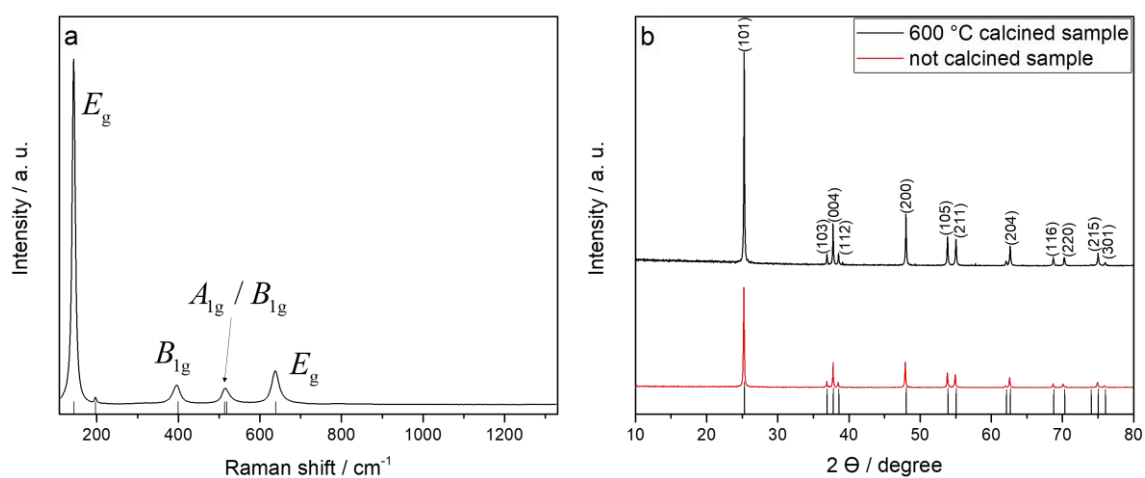


**Figure S1:** a) Raman spectrum of as-prepared powder TiO<sub>2</sub> powder; the anatase spectrum exhibits six Raman-active modes: one A<sub>1g</sub>, two B<sub>1g</sub>, and three E<sub>g</sub>. b) XRD pattern of an as-prepared and 600 °C calcined sample.

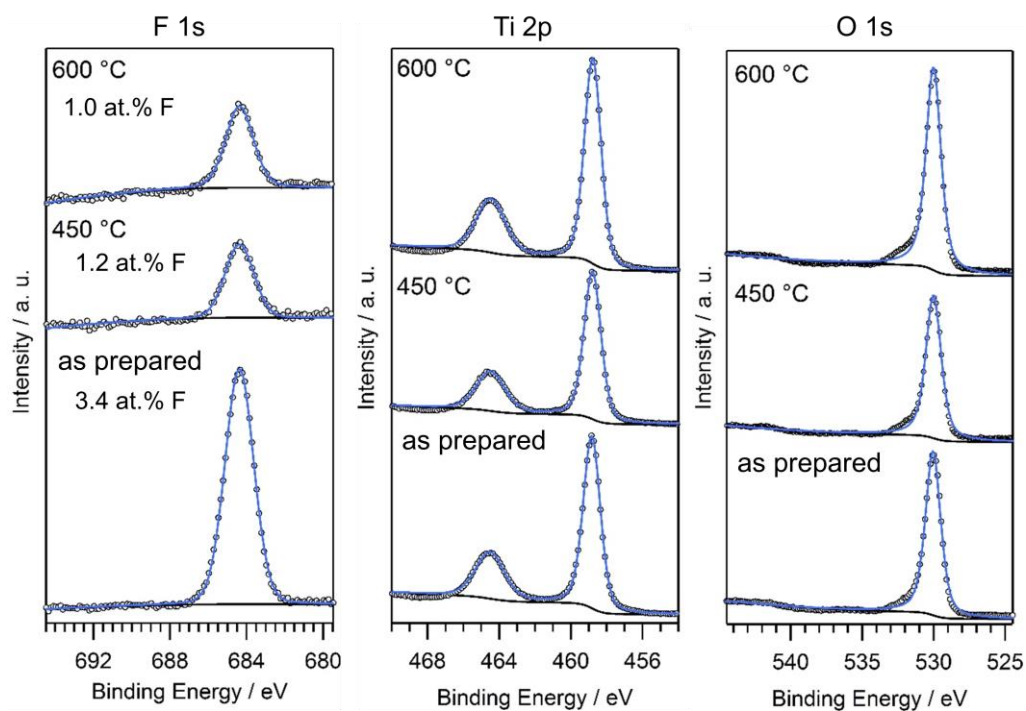


**Figure S2:** High-resolution XPS spectra of the F 1s, Ti2p and O 1s region of the as-prepared anatase crystals, and anatase crystals heated at 450°C and 600 °C for two hours. The circles represent the raw data, the blue and black lines represent the fitted and baseline, respectively.

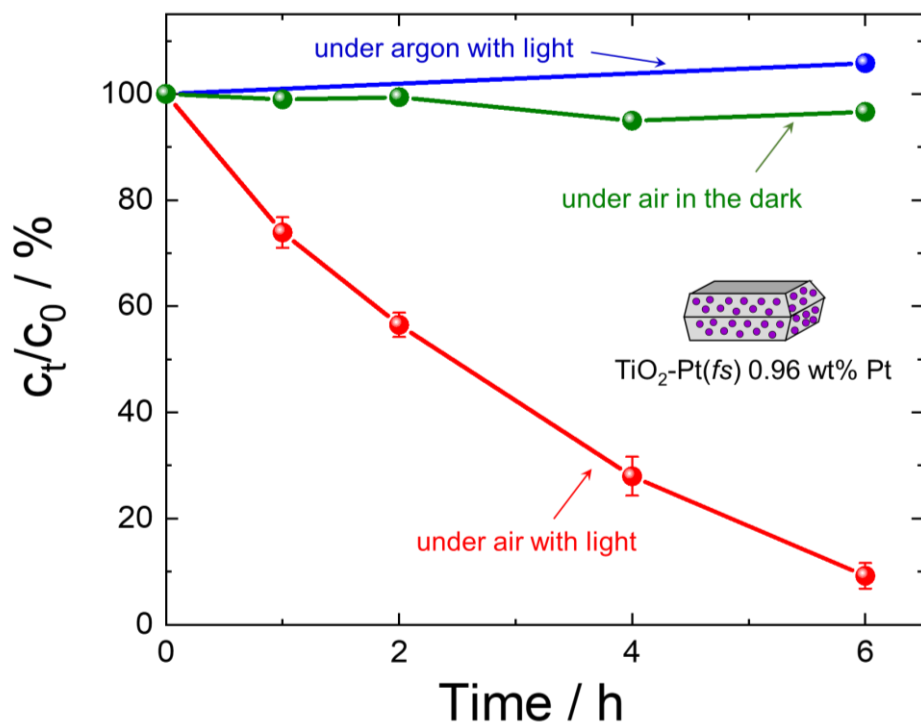


**Figure S3:** Blank 4-CP degradation experiments (in the dark; under argon + irradiation) performed with the best performing  $\text{TiO}_2\text{-Pt}(fs)$  (0.96 wt% Pt).

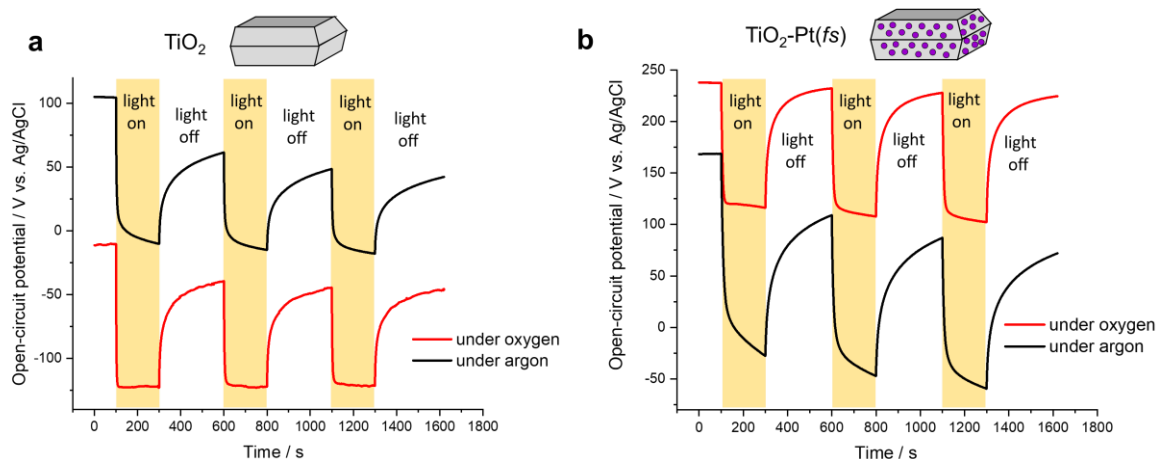


**Figure S1:** Open-circuit potential transients recorded under interrupted monochromatic illumination ( $\lambda = 350$  nm) for  $\text{TiO}_2$  (a) and  $\text{TiO}_2\text{-Pt}(fs)$  crystals (b) pressed onto Ti foil. The transients were recorded in 0.1 M  $\text{Na}_2\text{SO}_4$  (pH 7) under oxygen atmosphere (bubbling with  $\text{O}_2$  for 20 min) and in an oxygen-free environment (bubbling with Ar for 30 min). The electrodes were irradiated from the front-side.

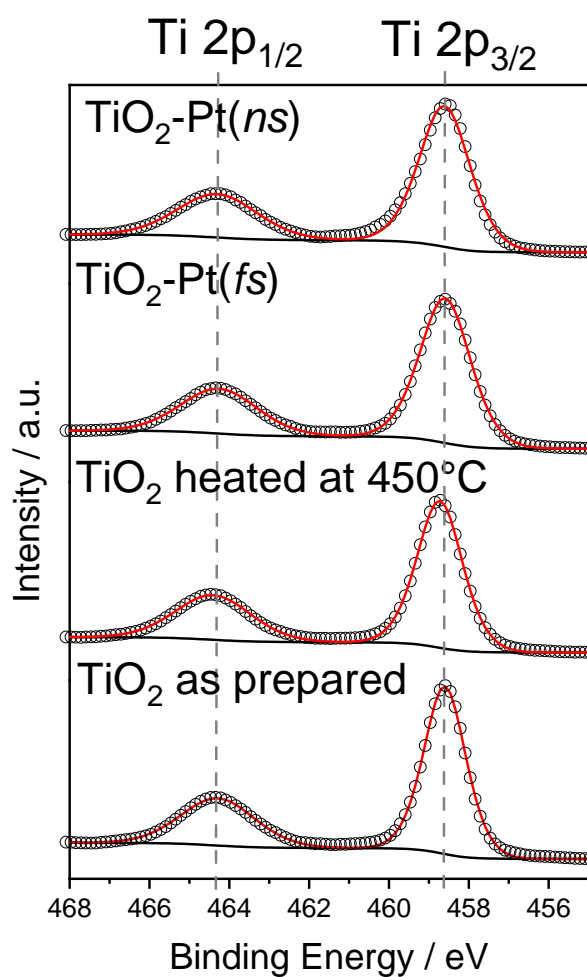


**Figure S5:** High-resolution XP spectra of the Ti2p region of the as-prepared anatase crystals and anatase crystals heated at  $450^\circ\text{C}$  without and with deposited Pt.